Long Spin Diffusion Length in Few-Layer Graphene Flakes

W. Yan,[1,*] L. C. Phillips,[1] M. Barbone,[2] S. J. Hämäläinen,[3] A. Lombardo,[2] M. Ghidini,[1,4] X. Moya,[1]
F. Maccherozzi,[5] S. van Dijken,[3] S. S. Dhesi,[5] A. C. Ferrari,[2] and N. D. Mathur[1,†]

[1]*Department of Materials Science, University of Cambridge, Cambridge CB3 0FS, United Kingdom*
[2]*Cambridge Graphene Centre, University of Cambridge, Cambridge CB3 0FA, United Kingdom*
[3]*NanoSpin, Department of Applied Physics, Aalto University School of Science, P.O. Box 15100, FI-00076 Aalto, Finland*
[4]*DiFeST, University of Parma, viale G.P. Usberti 7/A, 43124 Parma, Italy*
[5]*Diamond Light Source, Chilton, Didcot, Oxfordshire OX11 0DE, United Kingdom*
(Received 11 April 2016; revised manuscript received 29 June 2016; published 27 September 2016)

We report a spin valve with a few-layer graphene flake bridging highly spin-polarized $La_{0.67}Sr_{0.33}MnO_3$ electrodes, whose surfaces are kept clean during lithographic definition. Sharp magnetic switching is verified using photoemission electron microscopy with x-ray magnetic circular dichroism contrast. A naturally occurring high interfacial resistance ~ 12 MΩ facilitates spin injection, and a large resistive switching (0.8 MΩ at 10 K) implies a 70–130 μm spin diffusion length that exceeds previous values obtained with sharp-switching electrodes.

Graphene is at the center of an ever-growing research effort, due to its unique properties [1]. In particular, it shows great potential in spintronics [2–5], because its spin diffusion length l_{sf}^G is expected to be long compared to semiconductors and metals, as a consequence of weak spin-orbit coupling and weak hyperfine interaction [4,6]. Significant progress has been made towards the realization of spintronic devices [5], but a better understanding of spin transport in graphene is required in order to realize logic and memory operations in which the spin degree of freedom is manipulated [7,8]. Here we show that graphene possesses a spin diffusion length that is long (70–130 μm).

Spin transport has been previously measured in graphene [2,9–12], graphite flakes [13–16], and hexagonal boron nitride-encapsulated graphene [17]. By fitting Hanle curves [2] that describe the precession of transport spins in an out-of-plane magnetic field, a wide range of values for l_{sf}^G was reported, from 1 μm [15] up to 30 μm [17] at room temperature. The origin of the spin relaxation that limits l_{sf}^G is still debated and may be associated with impurities [18], ripples [6], substrates [19], and spin absorption in ferromagnetic electrodes [12,20,21].

Unwanted spin absorption arises in ferromagnetic electrodes if there is a "conductivity mismatch" with respect to a nonmagnetic channel, i.e., a discrepancy in the product of resistivity and spin diffusion length [22,23]. This problem can be avoided by inserting an insulating barrier between the two materials [23], e.g., with resistances in the range of a few MΩ for graphene with metallic electrodes [20]. By exploiting this approach, Ref. [3] reported $l_{sf}^G \sim 150$ μm in multilayer graphene, with the interfacial resistance (tens of MΩ) dominating the channel resistance (~ 1 kΩ). However, the magnetoresistance (MR) data in Ref. [3] showed quasicontinuous switching, incompatible with the parallel and antiparallel magnetic electrode configurations that were assumed when analyzing these data. Therefore, the reported value of l_{sf}^G may include contributions unrelated to spin transport, e.g., from tunneling anisotropic magnetoresistance (TAMR), which arises at contacts due to non-180° magnetic switching [24,25].

Here we demonstrate spin transport in a mechanically exfoliated flake of five-layer graphene (5LG), which bridges two epitaxial electrodes of the ferromagnetic oxide $La_{0.67}Sr_{0.33}MnO_3$ (LSMO) to form an LSMO-5LG-LSMO spin valve. At 10 K, this device can be switched using a magnetic field to interconvert the low state of resistance R_P with the high state of resistance $R_{AP} = R_P + \Delta R$, which is visible above the background noise ($\Delta R \sim 0.8$ MΩ, MR $= \Delta R / R_P \sim 3.0\%$). By contrast, previous reports based on these materials recorded no MR [26], or TAMR without spin transport [25]. Allowing the interfacial spin polarization γ to assume a plausible range of values $0.95 > \gamma > 0.54$ (as for Ref. [27]), the drift-diffusion model confirms long-distance spin transport at 10 K, with 70 μm $< l_{sf}^G < 130$ μm.

The required switching between parallel and antiparallel magnetic electrode configurations is confirmed at 150 K, using photoemission electron microscopy (PEEM) with magnetic contrast from x-ray magnetic circular dichroism (XMCD) [28]. Magneto-optical Kerr effect (MOKE) microscopy confirms that our uniaxial in-plane magnetic easy axis does not undergo any reorientation on cooling to the transport measurement temperature of 10 K. Therefore, our signal is due to spin transport, as intended.

The long spin diffusion length can be explained as follows. First, LSMO has a high spin polarization of up to 100% at 5 K [29,30] (and is therefore commonly used in spintronic devices [27,31]). Second, our LSMO surfaces are kept clean during electrode definition with a temporary layer

of Au, which is completely removed by chemical etching prior to few-layer graphene (FLG) transfer. Third, by adopting the pseudocubic (110) orientation of LSMO, we are able to switch between parallel and antiparallel magnetic electrode configurations at distinct and well-defined magnetic fields, which is nontrivial for complex oxides [32]. This sharp switching is essential for estimating l_{sf}^{G} without spurious effects, such as TAMR. Moreover, switching between single-domain states enhances spin signals [32]. Fourth, the insulating barriers required for good spin injection arise naturally from the structural and chemical discrepancy between the two materials. Fifth, flakes of FLG, whose physical properties represent an interpolation between two-dimensional single-layer graphene (SLG) and bulk graphite [33], possess larger values of l_{sf}^{G} than SLG, due to increased screening from impurity scattering potentials [13–15].

Sample preparation is as follows. Two similar LSMO films are grown epitaxially by pulsed laser deposition (PLD) on unterminated single crystals of $SrTiO_3$ (STO) (110) (as described in Supplemental Material [34]). The film used for the device and the MOKE studies is 30 nm thick. The film used for PEEM is slightly thicker (65 nm). Both have cube-on-cube epitaxy, are fully strained, and have atomically flat surfaces between step terraces (Supplemental Figs. S1 and S2 [34]). Vibrating sample magnetometry shows in-plane uniaxial magnetic anisotropy [41] collinear with $[001]_{STO}$. The anisotropy constant is $43\ kJ\,m^{-3}$ at 150 K and $6.5\ kJ\,m^{-3}$ at room temperature, similar to previous reports [42].

Similar electrodes are defined in both films by optical lithography and Ar-ion milling. For the PEEM sample, we avoid arcing by replacing the overmilled LSMO with 50 nm of sputter-deposited Au (using the electrode-definition mask as a lift-off mask prior to dissolution). For the spin-valve device, also used for MOKE, we (i) reduce any tendency for 5LG to sag by replacing the overmilled LSMO with 48 nm of amorphous $NdGaO_3$ (NGO) deposited at room temperature by PLD (again, using the electrode-definition mask as a lift-off mask prior to dissolution), (ii) ensure clean electrode surfaces by evaporating a 10-nm-thick protective Au layer prior to lithography, removing this layer in an aqueous KI/I_2 solution after lithography and then wiping with cotton buds soaked in isopropanol, and (iii) anneal in 55 kPa O_2 at 750 °C to avoid substrate conductivity.

FLG flakes are produced by micromechanical cleavage of natural graphite. A combination of optical contrast [35], Raman spectroscopy [36,37], and atomic force microscopy (AFM) is used to identify 5LG flakes. These are then transferred onto LSMO electrodes by a wet transfer technique [1,38] (see Supplemental Material [34]).

Magnetic switching of LSMO electrodes is studied at ~150 K using XMCD-PEEM (Fig. 1). The images are obtained at magnetic remanence after applying a magnetic field $\mu_0 H_{pulse}$ along the in-plane LSMO easy axis $\|[001]_{STO}$ (red arrow, Fig. 1). The value of XMCD asymmetry
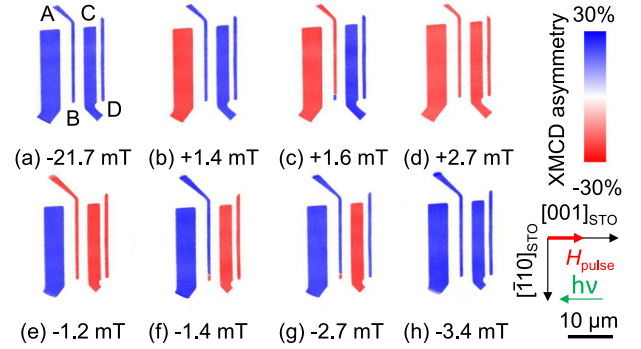
FIG. 1. Magnetic switching in LSMO (110) electrodes $A - D$ at 150 K. (a)–(h) PEEM images at remanence after applying a magnetic field $\mu_0 H_{pulse}$ along the LSMO easy axis $\|[001]_{STO}$ (red arrow). Field magnitudes represent upper bounds on the fields at which the observed switching occurs. XMCD asymmetry represents the projection of the in-plane surface magnetization on the in-plane projection of the grazing-incidence beam direction (green arrow). Blue (red) depicts magnetization parallel (antiparallel) to the green arrow. Transport is measured between B and C using similar electrodes.

represents the projection of the in-plane surface magnetization along the direction indicated by the green arrow (in-plane projection of the grazing-incidence beam) [32]. Regions of in-plane electrode magnetization lying parallel (antiparallel) to this green arrow appear blue (red). The initial application of a negative magnetic field leads to a homogeneously magnetized remanent state [Fig. 1(a)]. Successively larger positive field pulses lead to magnetization reversal in individual electrodes [Figs. 1(b) and 1(c)] and ultimately all four electrodes [Fig. 1(d)]. The subsequent application of successively larger negative field pulses leads to a second magnetization reversal in each electrode [Figs. 1(e)–1(h)].

The electrode switching sequence is, A, B, $C + D$ in the up sweep (Fig. 1(a–d)), and, A, B, D, C in the down sweep [Figs. 1(e)–(h)], differing only because the field steps in our up sweep are too large to distinguish switching in C and D. This switching sequence (widest, narrowest, narrowest, intermediate) is incompatible with the monotonic dependence of switching field on electrode width, as might be expected due to shape anisotropy. This suggests that there is a competition between more (fewer) nucleation sites and a lower (higher) demagnetizing field in wider (narrower) electrodes. The sharp switching, which we exploit for our spintronic devices, implies that domain-wall pinning is negligible, such that magnetization reversal is limited by domain nucleation.

MOKE microscopy is used to investigate magnetic switching in the widest LSMO electrode (A) at the 10 K magnetotransport measurement temperature (the sensitivity of the MOKE setup is not sufficient to reliably measure magnetic switching in the smaller electrodes). We find that the magnetic easy axis of electrode A is collinear with
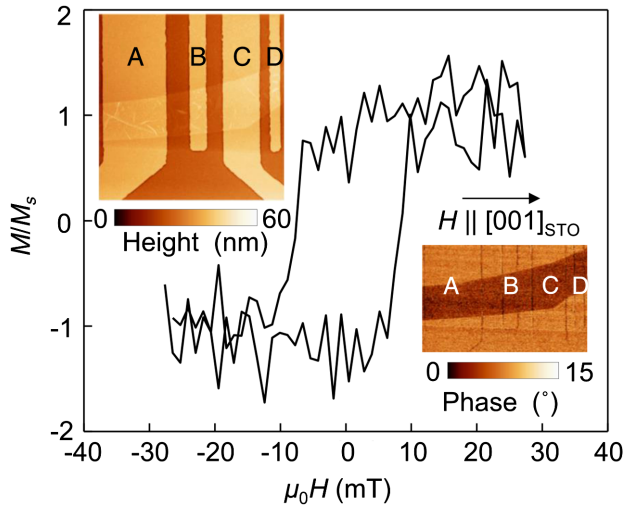
FIG. 2. LSMO-5LG-LSMO spin-valve characterization. MOKE microscopy measurements of magnetic switching in LSMO (110) electrode A at 10 K. The applied magnetic field $\mu_0 H$ and the measured component of magnetization M are collinear with the LSMO easy axis and $[001]_{STO}$. M_s is the saturation magnetization. The AFM image ($30~\mu m \times 30~\mu m$) (upper inset) and phase-contrast AFM image (lower inset) show the FLG flake.

$[001]_{STO}$ (Fig. 2), and the perpendicular in-plane direction is a magnetically anhysteretic hard axis. These MOKE observations are consistent with our 150 K imaging study of all four electrodes (Fig. 1). The magnitude of the electrode switching field measured by MOKE at 10 K ($|\mu_0 H| \sim 8$ mT, Fig. 2) exceeds the corresponding value that may be inferred from our imaging study at 150 K ($|\mu_0 H| \sim 1.2$–1.4 mT, Fig. 1), primarily because reducing the temperature increases the magnetic anisotropy, such that the nucleation field required for switching is higher [43].

The 5LG flake is positioned across all four LSMO electrodes $A - D$, as seen by AFM (upper inset, Fig. 2). The observed wrinkles are absent in a phase-contrast AFM image of the same area (lower inset, Fig. 2), implying that the flake is clean. The flake lies conformally on the LSMO electrodes, with sagging reduced due to the NGO deposited between electrodes.

Figure 3 compares the 5LG Raman spectra before and after transfer, confirming a successful transfer with no sample damage. The D peak is absent, implying a limited number of defects [35,37]. The Raman spectrum of the NGO-backfilled STO substrate (BSTO) (Fig. 3, green line) shows the expected peaks [44]. Since the D band of graphene and the $LO_4 + LO_2$ phonons of the BSTO substrate [44] both fall in a similar spectral range, the Raman spectrum of the BSTO substrate is subtracted point by point from the spectrum of 5LG on BSTO (Fig. 3, red line) to confirm that the D band remains absent after the transfer (Fig. 3, black line).

The two-terminal resistance between adjacent electrode pairs in the device at 10 K is $R_{AB} \sim 10$ MΩ, $R_{BC} \sim 24$ MΩ,
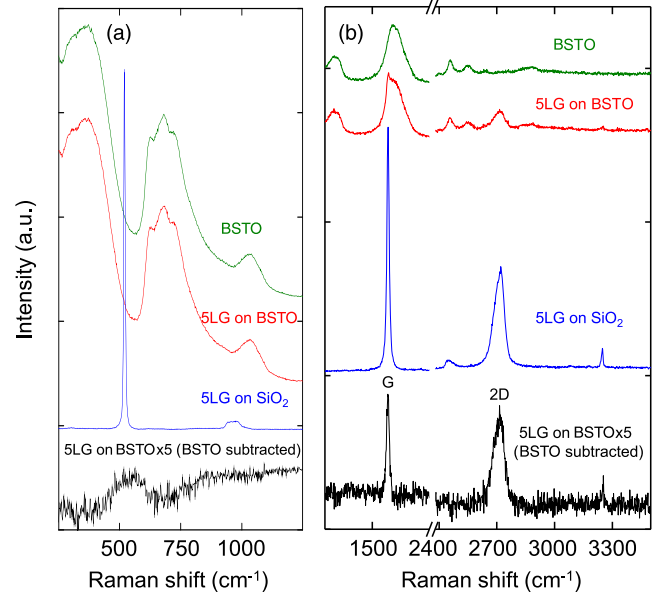
FIG. 3. (a,b) Raman spectra before and after 5LG transfer to LSMO electrodes separated the by NGO-backfilled STO substrate (BSTO). The Raman measurements after transfer are performed on the 5LG flake directly above the BSTO. The G and 2D peaks are visible for the flake on SiO_2 (blue) and after subsequent transfer to the LSMO electrodes separated by BSTO (red). A point-by-point subtraction of the BSTO background (green) yields the spectrum for the graphene flake on BSTO (black), where the D peak is absent.

and $R_{CD} \sim 150$ MΩ (electrode spacings $l_{AB} \sim 3~\mu m$, $l_{BC} \sim 2~\mu m$, and $l_{CD} \sim 1~\mu m$). Parasitic conduction through the substrate is excluded by measuring LSMO electrode pairs without 5LG, elsewhere on the same chip. The high values of resistance indicate that the LSMO-5LG interfaces function as tunnel barriers [25], consistent with nonlinear current-voltage plots (Supplemental Fig. S3 [34]). Device resistance is dominated by these LSMO-5LG interfaces, whose resistance-area products vary by an order of magnitude. This variation implies inhomogeneous interfacial transport, possibly with local current densities that produce failure in a region too small or too deeply buried for AFM detection.

Measurements of $R_{BC}(H)$ at 10 K are obtained during three full cycles of an applied magnetic field prior to device failure (Fig. 4, raw data in Supplemental Fig. S4 [34]). These data follow from measurements of over 20 devices. The noise may arise at the LSMO-5LG interfaces because of intermittent contact, or electrochemical reactions induced by Joule heating. Magnetically induced switching due to spin-valve behavior produces two symmetric high-resistance plateaux in the range 12.5 mT $< |\mu_0 H| < 34.5$ mT [Fig. 4(b)]. Given the switching sequence seen in Fig. 1 at the higher temperature of 150 K, we infer that B switches at the lower field ($|\mu_0 H_B| \sim 12.5$ mT), while C switches at the higher field ($|\mu_0 H_C| \sim 34.5$ mT), with higher
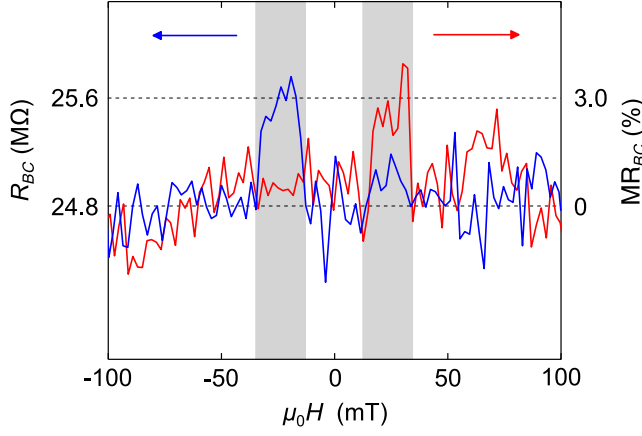
FIG. 4. LSMO-5LG-LSMO spin-valve magnetotransport at
10 K. Resistance R_{BC} and magnetoresistance MR_{BC} on decreas-
ing (blue) and increasing (red) magnetic field H along the
LSMO easy axis collinear with $[001]_{STO}$. Dashed lines indicate
$R_{BC} = 24.8$ MΩ and $R_{BC} + \Delta R_{BC} = 25.6$ MΩ for parallel and
antiparallel electrode magnetizations, respectively. The antipar-
allel configuration is indicated by gray shading in
12.5 mT $< |\mu_0 H| <$ 34.5 mT. Data obtained by averaging three
up and down sweeps (Supplemental Fig. S4). Bias voltage =
80 mV. 5LG bridges a 2 μm gap between electrodes B and C,
whose subscripts are dropped for analysis.

FIG. 5. LSMO-5LG-LSMO spin-valve parameters at 10 K.
Contours and grayscale show $MR(\gamma, l_{sf}^G)$ from the drift-diffusion
model [23]. For MR $\sim 3.0\%$ and $0.95 > \gamma > 0.54$, we find
70 μm $< l_{sf}^G <$ 130 μm (red contour). The red dot denotes
$MR(\gamma = 0.8, l_{sf}^G = 85 \ \mu\text{m}) = 3.0\%$ for the experimental value
of $R_P = 24.8$ MΩ. Inset: $MR(R_P)$ for $\gamma = 0.8$ and $l_{sf}^G = 85 \ \mu$m.

switching-field values at the lower temperature due
to enhanced uniaxial magnetic anisotropy [41].

The two high-resistance states at 10 K differ from the
low-resistance state $R_P = 24.8$ MΩ by $\Delta R \sim 0.8 \pm 0.2$ MΩ
(Fig. 4) (B and C subscripts are dropped for analysis).
This yields low-field MR $\sim (3.0 \pm 0.2)\%$. Given that
our electrodes display sharp 180° magnetization reversal
(Figs. 1 and 2), we deduce that the high-resistance states
arise from spin transport through the 5LG, rather than
TAMR or other effects linked to inhomogeneous magneti-
zation. This spin transport at 10 K may be interpreted using
the drift-diffusion model [23]:

$$\Delta R = \frac{2(\beta_{LSMO} R_{LSMO} + \gamma r_b^*)^2}{(r_b^* + R_{LSMO}) \cosh\left(\frac{L}{l_{sf}^G}\right) + \frac{R_G}{2}\left[1 + \left(\frac{r_b^*}{R_G^s}\right)^2\right]\sinh\left(\frac{L}{l_{sf}^G}\right)},$$

where $R_{LSMO} = (1/1 - \beta_{LSMO}^2)(\rho_{LSMO} l_{sf}^{LSMO}/wd)$ is the
spin resistance of LSMO, $R_G^s = \rho_s^G(l_{sf}^G/w)$ is the 5LG spin
resistance, $r_b^* = [R_P/2(1 - \gamma^2)]$ is the spin resistance
of each LSMO-5LG interface (whose resistance $R_P/2 \sim$
12 MΩ dominates the device resistance), β_{LSMO} is the bulk
LSMO spin polarization, γ is the interfacial spin polariza-
tion, l_{sf}^{LSMO} is the LSMO spin diffusion length, ρ_{LSMO} is the
LSMO resistivity, d is the width that we assume for both
LSMO electrodes separated by L, and w is the width of the
5LG flake with sheet resistance ρ_s^G.

Allowing the unknown parameters l_{sf}^G and γ to vary over
a wide range of values, we plot contours of MR $= \Delta R/R_P$
at 10 K (Fig. 5) using $R_P = 24.8$ MΩ [Fig. 4(b)],
$\beta_{LSMO} = 0.95$ [29], $l_{sf}^{LSMO} \approx 2.6$ nm [34] much smaller

than l_{sf}^G and therefore not critical, $\rho_{LSMO} = 10^{-6}$ Ωm as
measured for our films, $d = 6 \ \mu$m, $w = 7 \ \mu$m, and $\rho_s^G \approx$
400 Ω for our 5LG. If we assume $0.95 > \gamma > 0.54$ from
spin-polarized tunneling studies of LSMO [30,45], then
the contour representing MR $= 3.0\%$ is shallow, such that
l_{sf}^G at 10 K lies in a narrow range between 70 ($\gamma = 0.95$)
and 130 μm ($\gamma = 0.54$). Assuming $\gamma = 0.8$ as in Ref. [27]
implies $l_{sf}^G \sim 85 \ \mu$m (red dot, Fig. 5).

At higher temperatures, our 10 K values of 70 μm $\leq$
$l_{sf}^G \leq 130 \ \mu$m should not fall significantly given that l_{sf}^G has
been reported to show a weak temperature dependence in
both experimental [2,9,15] and theoretical [19] studies.
Therefore, we may directly compare our low-temperature
values with the smaller experimental values of $\leq$30 μm,
for graphitic flakes [13–15] and graphene [17] at various
temperatures, including room temperature. Although high
interfacial resistance is required to limit spin absorption
[12,20,21] in our LSMO electrodes, our interfacial resis-
tance is so high that MR is suppressed. This is seen for the
aforementioned choice of $\gamma = 0.8$, where reducing the
interfacial resistance to obtain $R_P = 12.5$ kΩ would
increase MR to 170% (Fig. 5, inset).

Increasing MR is attractive for applications [46], because
it leads to an increase of spin signal $V \times$ MR, i.e., the
voltage difference between parallel and antiparallel con-
figurations, when working at constant current (V is our bias
voltage). Our experimental MR $= 3.0\%$ with $V = 80$ mV
implies $V \times$ MR $= 2.4$ mV, whereas increasing MR to
170% would increase $V \times$ MR to 136 mV, exceeding the
LSMO-MWNT-LSMO value of 65 mV deemed suitable for

applications [27]. Note that our entire range $70\,\mu m \leq l_{sf}^G \leq 130\,\mu m$ exceeds the $50\,\mu m$ deduced for MWNTs [27], possibly reflecting different sources of spin relaxation [47], e.g., FLG edges and MWNT curvature.

In summary, we have reported spin transport at 10 K through a five-layer graphene flake that forms resistive interfaces with highly spin-polarized LSMO (110) electrodes, using XMCD-PEEM imaging to confirm sharp magnetic switching in the electrodes. By assuming $0.95 > \gamma > 0.54$, we infer values of $70\,\mu m < l_{sf}^G < 130\,\mu m$ that exceed previous experimental values for graphitic flakes [13–15] and graphene [17] with sharp-switching electrodes (note that l_{sf}^G has been reported to show a weak temperature dependence [2,9,15,19]). The key future challenge is to increase MR by reducing interfacial resistance, but annealing in forming gas [48] or using a current [49] would degrade the LSMO. Dry graphene transfer [50] could yield the desired reduction while also increasing l_{sf}^G through increased cleanliness.

---

*Present address: CIC nanoGUNE Consolider, Tolosa Hiribidea 76, E-20018 Donostia—San Sebastian, Spain.
†ndm12@cam.ac.uk

[1] A. C. Ferrari *et al.*, Nanoscale **7**, 4598 (2015).
[2] N. Tombros, C. Jozsa, M. Popinciuc, H. T. Jonkman, and B. J. van Wees, Nature (London) **448**, 571 (2007).
[3] B. Dlubak, M.-B. Martin, C. Deranlot, B. Servet, S. Xavier, R. Mattana, M. Sprinkle, C. Berger, W. A. de Heer, F. Petroff, A. Anane, P. Seneor, and A. Fert, Nat. Phys. **8**, 557 (2012).
[4] D. Pesin and A. H. MacDonald, Nat. Mater. **11**, 409 (2012).
[5] W. Han, R. K. Kawakami, M. Gmitra, and J. Fabian, Nat. Nanotechnol. **9**, 794 (2014).
[6] D. Huertas-Hernando, F. Guinea, and A. Brataas, Phys. Rev. Lett. **103**, 146801 (2009).
[7] S. Datta and B. Das, Appl. Phys. Lett. **56**, 665 (1990).
[8] B. Behin-Aein, D. Datta, S. Salahuddin, and S. Datta, Nat. Nanotechnol. **5**, 266 (2010).
[9] T.-Y. Yang, J. Balakrishnan, F. Volmer, A. Avsar, M. Jaiswal, J. Samm, S. R. Ali, A. Pachoud, M. Zeng, M. Popinciuc, G. Güntherodt, B. Beschoten, and B. Özyilmaz, Phys. Rev. Lett. **107**, 047206 (2011).
[10] I. Neumann, M. V. Costache, G. Bridoux, J. F. Sierra, and S. O. Valenzuela, Appl. Phys. Lett. **103**, 112401 (2013).
[11] M. V. Kamalakar, C. Groenveld, A. Dankert, and S. P. Dash, Nat. Commun. **6**, 6766 (2015).
[12] F. Volmer, M. Drögeler, E. Maynicke, N. von den Driesch, M. L. Boschen, G. Güntherodt, C. Stampfer, and B. Beschoten, Phys. Rev. B **90**, 165403 (2014).
[13] Y. Gao, Y. J. Kubo, C.-C. Lin, Z. Chen, and J. Appenzeller, in Proceedings of the 2012 IEEE International Electron Devices Meeting (IEDM) (unpublished), p. 4.4.1.
[14] H. Goto, A. Kanda, T. Sato, S. Tanaka, Y. Ootuka, S. Odaka, H. Miyazaki, K. Tsukagoshi, and Y. Aoyagi, Appl. Phys. Lett. **92**, 212110 (2008).
[15] T. Maassen, F. K. Dejene, M. H. D. Guimarães, C. Józsa, and B. J. van Wees, Phys. Rev. B **83**, 115410 (2011).
[16] M. Shiraishi, M. Ohishi, R. Nouchi, N. Mitoma, T. Nozaki, T. Shinjo, and Y. Suzuki, Adv. Funct. Mater. **19**, 3711 (2009).
[17] M. Drögeler, C. Franzen, F. Volmer, T. Pohlmann, L. Banszerus, M. Wolter, K. Watanabe, T. Taniguchi, C. Stampfer, and B. Beschoten, Nano Lett. **16**, 3533 (2016).
[18] K. Pi, W. Han, K. M. McCreary, A. G. Swartz, Y. Li, and R. K. Kawakami, Phys. Rev. Lett. **104**, 187201 (2010).
[19] C. Ertler, S. Konschuh, M. Gmitra, and J. Fabian, Phys. Rev. B **80**, 041405 (2009).
[20] H. Idzuchi, A. Fert, and Y. Otani, Phys. Rev. B **91**, 241407(R) (2015).
[21] M. V. Kamalakar, A. Dankert, J. Bergsten, T. Ive, and S. P. Dash, Sci. Rep. **4**, 6146 (2014).
[22] G. Schmidt, D. Ferrand, L. W. Molenkamp, A. T. Filip, and B. J. van Wees, Phys. Rev. B **62**, R4790 (2000).
[23] A. Fert and H. Jaffrès, Phys. Rev. B **64**, 184420 (2001).
[24] C. Gould, C. Rüster, T. Jungwirth, E. Girgis, G. M. Schott, R. Giraud, K. Brunner, G. Schmidt, and L. W. Molenkamp, Phys. Rev. Lett. **93**, 117203 (2004).
[25] L. C. Phillips, A. Lombardo, M. Ghidini, W. Yan, S. Kar-Narayan, S. J. Hämäläinen, M. Barbone, S. Milana, S. van Dijken, A. C. Ferrari, and N. D. Mathur, Appl. Phys. Lett. **108**, 112405 (2016).
[26] M. Rocci, J. Tornos, A. Rivera-Calzada, Z. Sefrioui, M. Clement, E. Iborra, C. Leon, and J. Santamaria, Appl. Phys. Lett. **104**, 102408 (2014).
[27] L. E. Hueso, J. M. Pruneda, V. Ferrari, G. Burnell, J. P. Valdés-Herrera, B. D. Simons, P. B. Littlewood, E. Artacho, A. Fert, and N. D. Mathur, Nature (London) **445**, 410 (2007).
[28] C. M. Schneider and G. Schönhense, Rep. Prog. Phys. **65**, R1785 (2002).
[29] J.-H. Park, E. Vescovo, H.-J. Kim, C. Kwon, R. Ramesh, and T. Venkatesan, Nature (London) **392**, 794 (1998).
[30] M. Bowen, A. Barthélémy, M. Bibes, E. Jacquet, J.-P. Contour, A. Fert, F. Ciccacci, L. Duò, and R. Bertacco, Phys. Rev. Lett. **95**, 137203 (2005).
[31] V. Garcia, M. Bibes, L. Bocher, S. Valencia, F. Kronast, A. Crassous, X. Moya, S. Enouz-Vedrenne, A. Gloter, D. Imhoff, C. Deranlot, N. D. Mathur, S. Fusil, K. Bouzehouane, and A. Barthélémy, Science **327**, 1106 (2010).
[32] L. C. Phillips, W. Yan, X. Moya, M. Ghidini, F. Maccherozzi, S. S. Dhesi, and N. D. Mathur, Phys. Rev. Applied **4**, 064004 (2015).
[33] A. H. Castro Neto, F. Guinea, N. M. R. Peres, K. S. Novoselov, and A. K. Geim, Rev. Mod. Phys. **81**, 109 (2009).
[34] See Supplemental Material at http://link.aps.org/supplemental/10.1103/PhysRevLett.117.147201, which includes Refs. [35–40], for details of fabrication, characterization and measurement, raw magnetotransport data, and calculation of the LSMO spin diffusion length.

[35] C. Casiraghi, A. Hartschuh, E. Lidorikis, H. Qian, H. Harutyunyan, T. Gokus, K. S. Novoselov, and A. C. Ferrari, Nano Lett. **7**, 2711 (2007).

[36] A. C. Ferrari, J. C. Meyer, V. Scardaci, C. Casiraghi, M. Lazzeri, F. Mauri, S. Piscanec, D. Jiang, K. S. Novoselov, S. Roth, and A. K. Geim, Phys. Rev. Lett. **97**, 187401 (2006).

[37] A. C. Ferrari and D. M. Basko, Nat. Nanotechnol. **8**, 235 (2013).

[38] F. Bonaccorso, A. Lombardo, T. Hasan, Z. Sun, L. Colombo, and A. C. Ferrari, Mater. Today **15**, 564 (2012).

[39] A. I. Lobad, R. D. Averitt, C. Kwon, and A. J. Taylor, Appl. Phys. Lett. **77**, 4025 (2000).

[40] A. Asamitsu and Y. Tokura, Phys. Rev. B **58**, 47 (1998).

[41] W. Yan, Ph.D. thesis, University of Cambridge, 2014.

[42] H. Boschker, J. Kautz, E. P. Houwman, G. Koster, D. H. A. Blank, and G. Rijnders, J. Appl. Phys. **108**, 103906 (2010).

[43] K.-D. Durst and H. Kronmüller, J. Magn. Magn. Mater. **68**, 63 (1987).

[44] W. G. Nilsen and J. G. Skinner, J. Chem. Phys. **48**, 2240 (1968).

[45] Y. Lu, X. W. Li, G. Q. Gong, G. Xiao, A. Gupta, P. Lecoeur, J. Z. Sun, Y. Y. Wang, and V. P. Dravid, Phys. Rev. B **54**, R8357 (1996).

[46] I. Žutić, J. Fabian, and S. Das Sarma, Rev. Mod. Phys. **76**, 323 (2004).

[47] D. Huertas-Hernando, F. Guinea, and A. Brataas, Phys. Rev. B **74**, 155426 (2006).

[48] M. Ishigami, J. H. Chen, W. G. Cullen, M. S. Fuhrer, and E. D. Williams, Nano Lett. **7**, 1643 (2007).

[49] T. Taychatanapat, Ph.D. thesis, Harvard University, 2013.

[50] B. Hunt, J. D. Sanchez-Yamagishi, A. F. Young, M. Yankowitz, B. J. LeRoy, K. Watanable, T. Taniguchi, P. Moon, M. Koshino, P. Jarillo-Herrero, and R. C. Ashoori, Science **340**, 1427 (2013).